



**HAL**  
open science

## **Giant magmatic water reservoirs at mid-crustal depth inferred from electrical conductivity and the growth of the continental crust**

Mickaël Laumonier, Fabrice Gaillard, Duncan Muir, Jon Blundy, Martyn Unsworth

### ► **To cite this version:**

Mickaël Laumonier, Fabrice Gaillard, Duncan Muir, Jon Blundy, Martyn Unsworth. Giant magmatic water reservoirs at mid-crustal depth inferred from electrical conductivity and the growth of the continental crust. *Earth and Planetary Science Letters*, 2017, 457, pp.173-180. <10.1016/j.epsl.2016.10.023>. <insu-01388434>

**HAL Id: insu-01388434**

**<https://insu.hal.science/insu-01388434v1>**

Submitted on 2 Nov 2016

**HAL** is a multi-disciplinary open access archive for the deposit and dissemination of scientific research documents, whether they are published or not. The documents may come from teaching and research institutions in France or abroad, or from public or private research centers.

L'archive ouverte pluridisciplinaire **HAL**, est destinée au dépôt et à la diffusion de documents scientifiques de niveau recherche, publiés ou non, émanant des établissements d'enseignement et de recherche français ou étrangers, des laboratoires publics ou privés.



Distributed under a Creative Commons CC BY-NC-SA 4.0 - Attribution - Non-commercial use - ShareAlike - International License

# Giant magmatic water reservoirs at mid-crustal depth inferred from electrical conductivity and the growth of the continental crust

## Authors (respecting order):

- 1- Mickael Laumonier<sup>1,2,3,4\*</sup> ([mickael.laumonier@gmail.com](mailto:mickael.laumonier@gmail.com)); [orcid.org/0000-0002-8816-6771](https://orcid.org/0000-0002-8816-6771),
- 2- Fabrice Gaillard<sup>2,3,4</sup> ([fabrice.gaillard@cnrs-orleans.fr](mailto:fabrice.gaillard@cnrs-orleans.fr)),
- 3- Duncan Muir<sup>5,6</sup> ([MuirD1@cardiff.ac.uk](mailto:MuirD1@cardiff.ac.uk)),
- 4- Jon Blundy<sup>5</sup> ([gljdb@bristol.ac.uk](mailto:gljdb@bristol.ac.uk)),
- 5- Martyn Unsworth<sup>7</sup> ([unsworth@ualberta.ca](mailto:unsworth@ualberta.ca)).

## Institutions:

<sup>1</sup>Bayerisches Geoinstitut, University of Bayreuth, 95440 Bayreuth, Germany.

<sup>2</sup>Université d'Orléans, ISTO, UMR 7327, 45071, Orleans, France.

<sup>3</sup>CNRS/INSU, ISTO, UMR 7327, 45071 Orléans, France.

<sup>4</sup>BRGM, ISTO, UMR 7327, BP36009, 45060 Orléans, France.

<sup>5</sup>School of Earth Sciences, University of Bristol, Bristol BS8 1RJ, UK.

<sup>6</sup>School of Earth and Ocean Sciences, Cardiff University, Cardiff CF10 3AT, UK.

<sup>7</sup>Department of Earth and Atmospheric Sciences, University of Alberta, Edmonton, Alberta, Canada.

\*Correspondence: M. Laumonier ([mickael.laumonier@gmail.com](mailto:mickael.laumonier@gmail.com)); (+33-473405591); mail: University B. Pascal / Laboratoire Magmas et Volcans / 6 avenue B. Pascal / 63178 AUBIERE Cedex

**One Sentence Summary:** Geophysical, laboratory conductivity and petrological experiments reveal that deep electrical conductivity anomalies beneath the Central Andes, Cascades and Taupo Volcanic Zone image the ponding of super-hydrous andesitic melts that contributes to the growth of continental crust.

**Abstract:**

The formation of the continental crust at subduction zones involves the differentiation of hydrous mantle-derived magmas through a combination of crystallization and crustal melting. However, understanding the mechanisms by which differentiation occurs at depth is hampered by the inaccessibility of the deep crust in active continental arcs. Here we report new high-pressure electrical conductivity and petrological experiments on hydrated andesitic melt from Uturuncu volcano on the Bolivian Altiplano. By applying our results to regional magnetotelluric data, we show that giant conductive anomalies at mid-crustal levels in several arcs are characterized by relatively low amounts of intergranular andesitic partial melts with unusually high dissolved water contents ( $\geq 8$  wt.% H<sub>2</sub>O). Below Uturuncu, the Altiplano-Puna Magma Body (APMB) displays an electrical conductivity that requires high water content (up to 10 wt.%) dissolved in the melt based on crystal-liquid equilibria and melt H<sub>2</sub>O solubility experiments. Such a super-hydrous andesitic melt must constitute about 10% of the APMB, the remaining 90% being a combination of magmatic cumulates and older crustal rocks. The crustal ponding level of these andesites at around 6 kb pressure implies that on ascent through the crust hydrous magmas reach their water saturation pressure in the mid-crust, resulting in decompression-induced crystallization that increases magma viscosity and in turn leads to preferential stalling and differentiation. Similar high conductivity features are observed beneath the Cascades volcanic arc and Taupo Volcanic Zone. This suggests that large amounts of water in super-hydrous andesitic magmas could be a common feature of active continental arcs and may illustrate a key step in the structure and growth of the continental crust.

**Keywords:** electrical conductivity; water; andesite; continental crust growth; arc magmas

## 1. Introduction

Convergent plate boundaries (subduction zones) are the loci of voluminous magmatism triggered by the release of volatiles, predominantly water, from the subducted plate into the overlying mantle and crust (Grove et al., 2012). Arc magmatism is widely considered to be the primary mechanism of continental crust formation, whereby mantle-derived magmas with basaltic to high-Mg andesitic compositions differentiate within the crust to produce more evolved, silica-rich magmas (e.g. Annen et al., 2006; Castro et al., 2013). However, within this conceptual petrological framework, ongoing uncertainty remains about many of the key details, hampering our understanding of the mechanisms of magmatic differentiation, crustal growth and water recycling through subduction zones. For example, although Earth's continental crust has an overall andesitic composition (Rudnick, 1995), it is unclear whether andesite is truly the most abundant melt composition above subduction zones (Carmichael, 2002; Castro et al., 2013), or whether magma mixing and crustal melting play an important role in producing the observed compositional spectrum (Reubi & Blundy, 2009; Lee & Bachmann, 2014; Laumonier et al., 2014; Keller et al., 2015). Similarly, there is uncertainty over the dissolved magmatic water and carbon dioxide contents of arc magmas and the role that they play in triggering volatile saturation (Blundy et al., 2010), driving compositional diversity (Melekhova et al., 2013) and controlling the depths at which magmas stall and differentiate (Annen et al., 2006; Blatter et al., 2013). Water contents up to 10 wt.% have been measured in andesite melt inclusions (Grove et al., 2012) and inferred from mineral chemistry (Edmonds et al., 2014), whereas most arc basalts appear to contain approximately 4 wt.% H<sub>2</sub>O (Plank et al., 2013). Although differentiation of hydrous basalts will tend to increase dissolved H<sub>2</sub>O contents, this is only possible at elevated pressures because of the depth-dependent solubility of volatiles. It is unclear whether very high water contents are representative of arc magmas or simply local anomalies resulting, for example, from relatively high-pressure differentiation.

The study of exhumed rocks can elucidate many ancient magmatic processes occurring close to the surface, although the effects of melt solidification and modification during exhumation can confer complications. To image magmatic processes in real time, or at greater depth, geophysical exploration, such as seismic or magnetotelluric (MT) surveys are required. By measuring the crustal-scale conductivity and seismic wave velocity, geophysical exploration has produced 3D images of subduction zone magmatic systems (Comeau et al., 2015; Hill et al., 2009; Ward et al., 2014; Heise et al., 2010). In principle, conductivity and seismic images are able to detect silicate melts in the process of solidification

to form plutonic rocks. Such images are not, however, unambiguous in their interpretation as a variety of interwoven factors can produce anomalies in velocity or conductivity. For example, electrical conductivity is sensitive to both the amount and the composition of the melt, including its dissolved water content, and also to pressure and temperature (Gaillard, 2004; Laumonier et al., 2015). The interpretation of MT data must be informed by laboratory studies of the electrical conductivity of melts at relevant pressure and temperature. To minimise ambiguity this interpretation must be placed in a petrological and geological context that includes the composition (and water content) of melt reservoirs and their distribution within the crust. In this study, we characterize the effects of temperature, pressure, dissolved water content and melt fraction to develop a model of electrical conductivity that can be used to interpret crustal conductivity anomalies due to andesitic partial melt. By combining our results with petrological experiments we are able to reveal the presence of large amounts of water dissolved in partial melts in mid crustal reservoirs formed by ponding of melts at their water-saturation depth.

## 2. Methods

### 2.1. Starting materials and hydration of samples

Samples for the electrical conductivity measurements were prepared from an andesitic inclusion (UTU5; Table 1) from Cerro Uturuncu, a Pleistocene volcano on the Bolivian Altiplano (Sparks et al., 2008). The andesite inclusions are hosted by dacite lava flows, which are the dominant eruptive product from Uturuncu. The andesites represent quenched intermediate magmas mixed into the dacites shortly before eruption (Sparks et al., 2008). A similar Uturuncu andesite sample was used in the phase equilibrium experiments (Table 1). The natural rock was crushed to powder and fused twice at atmospheric pressure to produce a homogeneous, volatile-free glass. This glass was used for both dry experiments and as the starting material for the hydration syntheses in a piston cylinder and internally heated pressure vessel as described in Laumonier et al. (2015).

	SiO <sub>2</sub>	TiO <sub>2</sub>	Al <sub>2</sub> O <sub>3</sub>	FeO	MgO	MnO	CaO	Na <sub>2</sub> O	K <sub>2</sub> O	Total
<b>GSM13N</b> (Muir et al. 2015)	56.5	1.3	16.3	7.7	5.8	nd	7.9	2.4	1.9	99.8
<b>UTU5</b> Sparks et al. (2008)	59,85	1,17	17,26	7,14	3,38	0,11	5,83	2,27	2,99	99,62
<b>Dry starting glass</b>	60,93 0,27	1,14 0,09	17,20 0,14	6,60 0,28	3,20 0,16	0,12 0,08	5,54 0,10	2,09 0,05	3,17 0,07	98,47 0,38

Exp. UTU5-15kb-0	61,46	1,15	17,10	6,37	3,27	0,01	5,51	2,10	3,02	98,34
	<i>0,20</i>	<i>0,08</i>	<i>0,14</i>	<i>0,20</i>	<i>0,06</i>	<i>0,02</i>	<i>0,06</i>	<i>0,03</i>	<i>0,04</i>	<i>0,19</i>
Exp. UTU5-15kb-1.8	61,37	1,18	17,79	5,82	3,31	0,03	5,31	2,17	3,03	96,65
	<i>0,67</i>	<i>0,08</i>	<i>0,53</i>	<i>0,20</i>	<i>0,17</i>	<i>0,03</i>	<i>0,14</i>	<i>0,09</i>	<i>0,10</i>	<i>0,34</i>
Exp. UTU5-15kb-5.9	61,08	1,17	17,21	6,27	3,40	0,09	5,48	2,11	3,19	92,78
	<i>0,46</i>	<i>0,12</i>	<i>0,30</i>	<i>0,46</i>	<i>0,60</i>	<i>0,11</i>	<i>0,19</i>	<i>0,07</i>	<i>0,10</i>	<i>0,24</i>
Exp. UTU5-15kb-7.2	61,75	1,23	18,38	4,89	3,30	0,01	5,37	2,03	3,03	91,19
	<i>0,77</i>	<i>0,09</i>	<i>0,66</i>	<i>0,16</i>	<i>0,10</i>	<i>0,01</i>	<i>0,14</i>	<i>0,03</i>	<i>0,06</i>	<i>0,34</i>

**Table 1: Chemical compositions of the starting material and experimental glasses from electrical conductivity measurements.** Standard deviations are indicated in the italic font below.

The water content in the glass was measured before and after the experiments with infra-red spectroscopy at ISTO (Microscope IR Continuum coupled with a Nicolet 6700 spectrometer and a MCT detector, Orleans, France) and BGI (Bruker IFS 120HR FTIR spectrometer, Bayreuth, Germany) using a KBr beam splitter. At least 128 scans with a resolution of  $4\text{ cm}^{-1}$  were carried out for each spectrum. Each sample was analysed through 7 to 25 spots to check for homogeneity of the water concentration. We used a linear baseline correction to determine the peak height absorbance, and calculated the water concentration by the Beer-Lambert law, using extinction coefficients for dacite with similar composition (Ohlhorst et al., 2001). The thickness of the sample was measured by a Mitutoyo digital micrometre and checked by the calibrated stage of the microscope. To minimize the uncertainty, samples were kept as thick as possible but transparent for IR rays (thickness  $< 200\ \mu\text{m}$ ). Depending on the water content, the sample thickness and transparency, either the fundamental  $\text{H}_2\text{O}$ -stretching vibration ( $3530\text{ cm}^{-1}$ ) or the molecular water ( $5200\text{ cm}^{-1}$ ) and OH- ( $4500\text{ cm}^{-1}$ ) stretching vibrations were used. The propagated uncertainty takes into account the accuracy of (i) the thickness, (ii) the absorbance peak height, (iii) glass density and (iv) extinction coefficient, resulting in a typical error in  $[\text{H}_2\text{O}]$  of 0.5 wt.%. After experiments, the samples were inspected to verify that the chemical composition of the glasses closely matched the starting material (Table 1) and the water content measured after experiments ranges between 1.7 and 9.0 wt. % (Fig. S3).

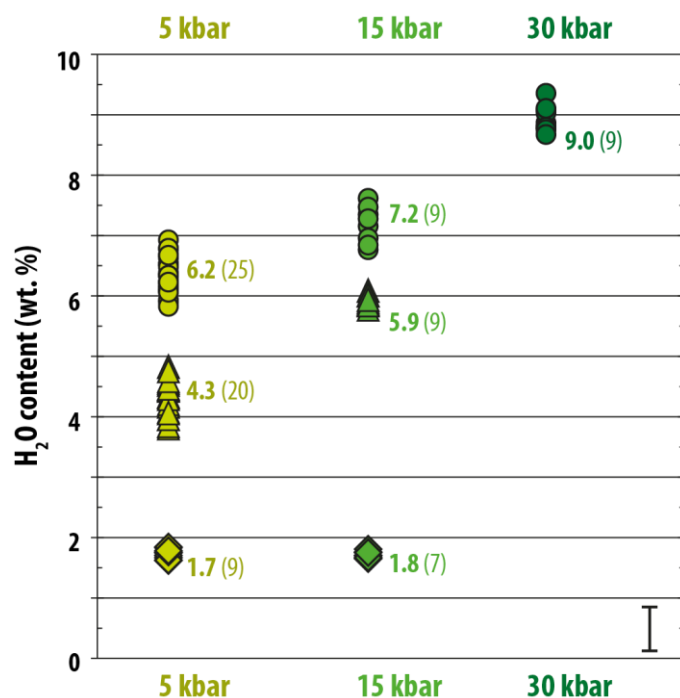


**Fig. 1: Water content analyses by FTIR of the glasses after experiments.** The number of analyses is indicated in brackets.

## 2.2. Electrical experiments

Ten *in situ* electrical conductivity experiments were conducted at three different pressures on the andesite glass with various water contents using a ½" and ¾" end-loaded piston cylinder apparatus at ISTO following the procedure of Sifré et al. (2014) and Laumonier et al. (2015) (Table 2). The background of the electrical conductivity of silicate melts is described elsewhere (e.g. Gaillard, 2004; Pommier et al., 2008; 2014; Laumonier et al., 2015). Electrical conductivity was determined from the sample resistance measured by impedance spectroscopy. Impedance data were acquired during repeated heating-cooling cycles in the temperature range where the sample is liquid (Fig. 2). The temperature was quickly increased (about 200°C/min) to ~1,100°C to minimize crystallization and water loss. To reduce the risk of sample dehydration, run durations were kept as short as possible (typically less than 3 hours; Table 2). The subsequent experimental procedure consisted of varying the furnace power using manual settings, followed by a 1-minute delay to allow equilibration of the sample before collecting electrical measurements. Conductivity was measured during at least two heating and one cooling cycles to ensure the reproducibility of the experiments. In general, the resistance of the sample was slightly higher during the first heating, while the second and third paths (cooling and 2<sup>nd</sup> heating) gave identical values (Fig. 2). Negligible (if any) modification of the sample dimensions and chemistry must have

occurred during the experiment given the reproducibility of the heating-cooling path resistance values and the constant resistance with time (error on the conductivity lower than 0.2 log units; [Laumonier et al., 2015](#)). After experiments, the samples were inspected to ensure the absence of crystals and to accurately determine the geometry of the sample.

Experiment #	Pressure (GPa)	H <sub>2</sub> O (wt.%)	G	T°C (1)	T°C (2)	Duration	Ea (J)	Log $\sigma_0$
UTU5-5kb-0	0.5	0.1	0.0212	1043	1289	3:59	139184	4.33
UTU5-5kb-1.7	0.5	1.7	0.0067	996	1231	2:42	129178	4.35
UTU5-5kb-4.3	0.5	4.3	0.0123	910	1141	1:59	92740	3.55
UTU5-5kb-6.2	0.5	6.2	0.0234	962	1213	2:36	82289	3.59
UTU5-15kb-0	1.5	0.0	0.0137	1366	1137	2:07	171202	5.37
UTU5-15kb-1.8	1.5	1.8	0.0129	1372	1149	2:37	151101	5.02
UTU5-15kb-5.9	1.5	5.9	0.0210	1465	1123	2:01	96602	4.01
UTU5-15kb-7.2	1.5	7.2	0.0225	1111	1407	1:21	78867	3.57
UTU5-30kb-0	2.8	0.0	0.0095	1027	1319	2:15	185478	5.63
UTU5-30kb-9.0	3.0	9.0	0.0088	1382	1153	1:39	67168	3.61

**Table 2: Experimental conditions of the electrical conductivity runs.** Water content determined by FTIR, G is the geometrical factor, T°C (1) and (2) are the limit temperature of the selected path use for modelling, duration in h:mm, Activation energy (Ea) and pre-exponential factor  $\sigma_0$  in S/m.

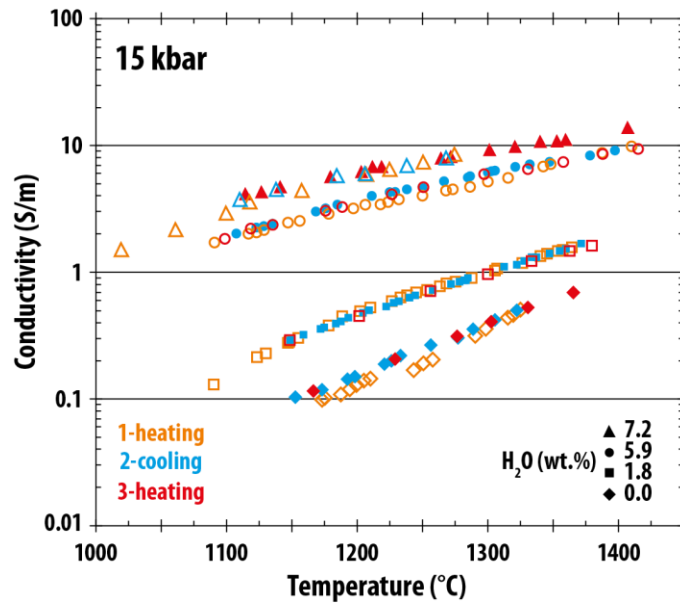


**Fig. 2: Temperature vs. electrical conductivity plot** showing the heating-cooling paths of experiments performed at 15 kbar and highlighting the reproducibility of the conductivity measurements.

### 2.3. Phase equilibrium experiments.

Volatile-saturated and under-saturated melting experiments were conducted at pressures from 5 to 8 kbar and temperatures from 890 to 980°C on andesite sample GSM13N (Table 1 & 3) (Muir et al., 2014a, b; 2015). Experiments were performed using a ½” end-loaded piston cylinder apparatus at the University of Bristol. Capsules were prepared and buffered with nickel-nickel oxide powders using the double capsule method of Jakobsson (2012). For volatile-saturated charges ~20 wt% H<sub>2</sub>O was added by pipette to the inner capsule; 4 to 7 wt% H<sub>2</sub>O was added to the volatile-undersaturated charges. A similar amount of H<sub>2</sub>O was added to the outer capsule along with the Ni-NiO buffer material. Capsules were weighed before and after welding to check for H<sub>2</sub>O loss. The hot piston-in technique (Boyd, 1960; Green & Ringwood, 1967) was employed with a friction correction of -3% (McDade et al., 2002) applied to all experiments. Motorised pressure controls on the piston cylinders ensure oil pressure remains constant during experimental runs. Temperature was measured using a programmable Eurotherm controller and a type D (W/Re) thermocouple with an estimated accuracy of ±2°C and was held within ±1°C of the set point for each experiment. Runs were quenched by switching off the power supply with resulting cooling rates in excess of 100°C per second. Major element chemistries of experimental run products were analysed by electron microprobe at the University of Bristol. Glass fraction was determined by mass balance.

Run #	Run conditions				Run Products		Plagioclase		H <sub>2</sub> O in melt			
	P (kb)	T (°C)	time (hours)	Initial wt. % H <sub>2</sub> O	Glass fraction	Minerals	An content	sd	SIMS	sd	VBD	sd
92-5U	5	920	97	5.1	0.62	plag,amph,ox	0.892	0.012	9.4	0.2		
98-5U	5	980	65	4.2	0.72	plag,cpx,opx,ox	0.770	0.017	7.3	0.1		
88-5U2	5	880	65	2.0	0.52	plag,amph,ox	0.655	0.044			5.38	0.35
89-5U	5	890	46	6.5	0.54	plag,amph,ox	0.827	0.037			8.79	0.62
95-5U	5	950	49	5.0	0.55	plag,amph,cpx,ox	0.823	0.069	8.3	0.6		
98-8U	8	980	48	4.9	0.63	plag,amph,opx,cpx	0.747	0.017	7.9	0.1		
88-8U2	8	880	66	1.8	0.52	plag,amph,opx,ox	0.659	0.036			5.86	0.85
92-8U	8	920	49	4.3	0.63	plag,amph,cpx,ox	0.827	0.072	8.3	0.8		

**Table 3: Experimental conditions of the phase equilibrium experiments.** plag: plagioclase; amph: amphibole; ox: oxides; cpx: clinopyroxene; opx: orthopyroxene, An: anorthite; sd: standard deviation; VBD: value By difference

Water contents of experimental glasses were analysed on a Cameca ims4f Secondary Ion Mass Spectrometer (SIMS) at the NERC ion microprobe facility (University of Edinburgh, UK). Samples were mounted in low-volatility resin and coated with a ~20 nm thick layer of Au. Experimental glass pools

>50  $\mu\text{m}$  were analysed with a 10 kV primary beam of  $\text{O}^-$  ions and a nominal beam current of 5 nA.  $\text{H}_2\text{O}$  was measured as  $^1\text{H}^+$  secondary ions from a pre-cleaned 25 micron image field with an extraction voltage of 4.5 kV and an offset of 75 V.  $\text{H}_2\text{O}$  was calibrated against glass standards NIST610, Sisson51, Lipari and MC84b2 containing 0.72 to 4.32 wt%  $\text{H}_2\text{O}$ . Calibration working curves of  $^1\text{H}/^{30}\text{Si}$  vs  $\text{H}_2\text{O}$  with  $R^2 > 0.99$  were used to calculate  $\text{H}_2\text{O}$  content. SIMS analysis sites were examined post-SIMS using a scanning electron microscope. Any analyses that visibly intersected crystals were discarded. The results of the phase equilibrium experiments are presented in section 4.1.1. Note that natural andesite phase assemblages with predominant plagioclase and orthopyroxene were reproduced in several runs.

### 3. Results and model of the electrical conductivity of andesite

The results of the electrical conductivity (EC) measurements are shown in Figure 3 (see also Table 2). The EC of the andesite melt increases with increasing temperature, and slightly decreases with increasing pressure. Most striking, however, is the dramatic increase in EC with water content (more than 100-fold between 0 and 9 wt.% water at 30 kbar; Figure 3).

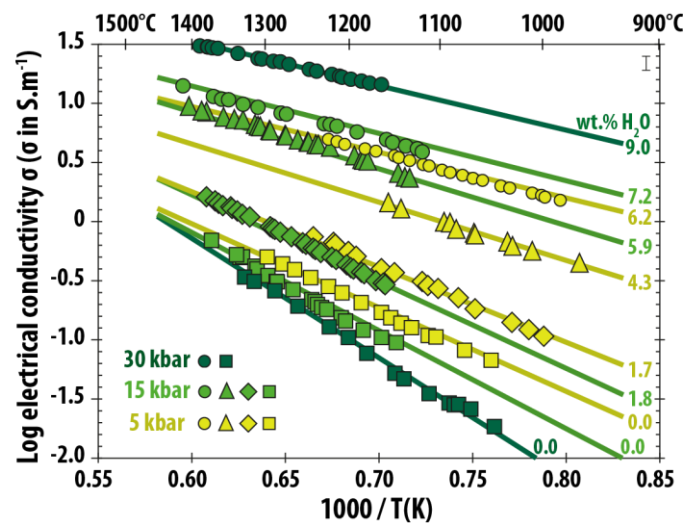


**Fig. 3.** *In situ* electrical conductivity as a function of temperature for an andesite melt with various water contents at pressures of 5, 15 and 30 kbar (symbols). Numbers on the right of the graph indicate the water contents. Fits to the data (lines) are calculated according to the model described in the text (Section 3).

The andesitic melt conductivity ( $\sigma_{\text{and}}$ ,  $\text{S}\cdot\text{m}^{-1}$ ) increases with temperature, following an Arrhenius law:

$$\sigma_{and} = \sigma_0 \cdot \exp^{-(Ea+P\Delta V)/RT} \quad (\text{eq. 1})$$

where  $\sigma_0$  is a pre exponential factor ( $\text{S}\cdot\text{m}^{-1}$ ),  $Ea$  the activation energy (J),  $P$  the pressure (bar),  $\Delta V$  the activation volume ( $\text{cm}^3\cdot\text{mol}^{-1}$ ),  $R$  the gas constant and  $T$  the temperature (K). Activation energy ranges from 171 kJ for dry melts to 67 kJ for the most hydrated samples and the logarithm of the pre-exponential factor  $\sigma_0$  depends linearly on the water content and the pressure (Fig. 4). These relationships were then used to build a conductivity model of andesite melt as a function of temperature, pressure and water content following the method of Laumonier et al. (2015):

$$\sigma_0 = \exp\{(aw + b) + P * (cw + d)\} \quad (\text{eq. 2})$$

$$Ea = ew + f \quad (\text{eq. 3})$$

$$\Delta V = gw + h \quad (\text{eq. 4})$$

where  $w$  is the water concentration in wt.%,  $P$  is the pressure in bars, and  $a$  to  $h$  are parameters determined by fitting (correlation coefficient = 0.998) the measured data (Table 4). The conductivity model reproduces the measured data with an average difference of 0.03 log units and is plotted along with the measurements (Fig. 3). Similar electrical properties (in particular the charge carrier  $\text{Na}^+$ ) are assumed in andesitic and felsic melts (Gaillard, 2004; Laumonier et al., 2015). The bulk conductivity of a magma (melt + crystals) can be calculated using our model and the modified Archie's law (Glover et al., 2000) with an exponent of 1.05 (Gaillard et Iacono-Marziano, 2005). We assume that the melt has an andesitic composition and is distributed through a solid matrix dominated by plagioclase and orthopyroxene ( $\sigma_{\text{plagioclase}} = 3.2\text{E-}4$  and  $\sigma_{\text{orthopyroxene}} = 1.3\text{E-}3$  at  $980^\circ\text{C}$ ; Maury, 1968). However, the exact mineralogy of the matrix has little bearing on our findings as minerals are substantially less conductive than the melts (about three orders of magnitude; Maury, 1968).

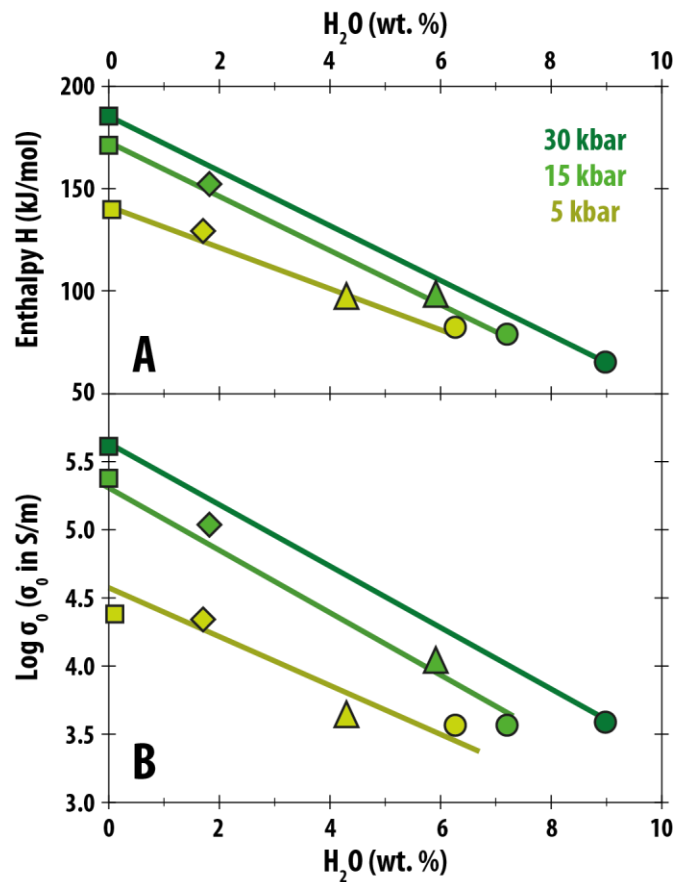


**Fig. 4:** Linear relationships between Enthalpy  $H$  ( $H = E_a + P\Delta V$ ) (A) and Logarithm of the pre-exponential factor  $\sigma_0$  (B) with water respectively, used to fit the data.

$\sigma_0$				$E_a$		$\Delta V$	
a	B	c	d	e	f	g	h
-0,34	8,96	-8,07E-06	1,67E-04	-9627	1,25E+05	-1,46E-01	2,462
<i>0,29</i>	<i>0,07</i>	<i>3,47E-06</i>	<i>1,79E-05</i>	<i>805,3</i>	<i>3,56E+03</i>	<i>4,20E-02</i>	<i>0,213</i>

**Table 4:** Parameters derived from the data fitting the equations (1) to (4) with standard deviation (italic font).  $\sigma_0$  is the pre-exponential factor ( $S.m^{-1}$ ),  $E_a$  is the activation energy ( $J.mol^{-1}$ ) and  $\Delta V$  is the activation volume ( $cm^3.mol^{-1}$ ).

## 4. Discussion

### 4.1. Determination of the water content and melt fraction in deep crustal reservoirs

Our data can be used to infer the amount of magma and water content of the deep crustal conductors detected by MT surveys in three different major, active continental arcs: Altiplano-Puna magma body (APMB) located in the central Andes; the Southern Washington Cascades Conductor beneath the

Cascade volcanic arc (SWCC; USA), and the conductor beneath the Taupo Volcanic Zone (TVZ; New Zealand) (Comeau et al., 2015; Hill et al., 2009; Heise et al., 2010; Wannamaker et al., 2014).

#### 4.1.1. Altiplano-Puna Magma Body

The Altiplano-Puna Magma Body (APMB) is located in the central Andes, the type example of an ocean-continent subduction zone. The APMB is arguably the largest crustal magma body identified on Earth (Zandt et al., 2003). Volcanism above the APMB is mostly dacitic, but andesite enclaves and noritic xenoliths are common and attest to the role of more mafic magmas in dacite petrogenesis along with mixing and crustal melting (Sparks et al., 2008; Muir et al., 2014; Michelfelder et al., 2014). The low seismic velocity and density of the APMB are consistent with a significant melt fraction that remains below 25 vol% (del Potro et al., 2013; Ward et al., 2014). Magnetotelluric studies show that the APMB comprises a layer at a depth of 20-35 km below the surface with relatively elevated conductivities ( $\sigma = 1 \text{ S m}^{-1}$ ) (Comeau et al., 2015). Both 2-D and 3-D inversions have been applied to these MT data and yield broadly similar models. It should be noted that MT determines the integrated conductivity, and the inversions are implemented to give the maximum conductivity that is consistent with the MT data. The geophysical characteristics (seismic, gravity, heat flow and electrical) of the AMPB have long been attributed to the presence of magmas. Saline fluids could generate the high conductivity of the APMB if they could connect over large distances (several 10s of km), though the geological process producing such a large amount of chlorine-rich fluid is unclear. Exsolution of magmatic volatiles from magma would produce high temperature, water-rich and chlorine-poor fluids, remaining as bubbles in the magma and therefore invisible to MT data.

The petrology of the Uturuncu andesite enclaves indicates pre-eruptive magma equilibration at temperatures of  $980 \pm 10^\circ\text{C}$  (Sparks et al., 2008). The andesites contain phenocrysts and microphenocrysts of calcic plagioclase (over  $\text{An}_{70}$ ) orthopyroxene and Fe-Ti oxides, with minor or rare clinopyroxene and amphibole in some inclusion (Sparks et al., 2008). The phenocrysts are thought to represent the phase assemblage of the andesite magma at depth, prior to mixing into the dacite host (Muir et al., 2014a). These observations can be used to interpret the high conductivity of the APMB in terms of melt fraction and water content assuming that the APMB contains andesitic melt similar to that in the enclaves. In this regard it is noteworthy that the phase equilibrium experiments best reproduce the natural plagioclase + orthopyroxene assemblage at  $980^\circ\text{C}$  and 5-8 kbar (Table 3), consistent with the depth to the APMB as determined geophysically. Uncertainties in temperature have

little effect on the conductivity since  $\log \sigma$  changes by  $\sim 0.1$  with a variation of  $50^\circ\text{C}$  at 6 kbar and  $\text{H}_2\text{O} = 7 \text{ wt.}\%$ . This demonstrates that the conductivity of andesite melt is controlled primarily by its dissolved water content. [Figure 5](#) shows the combination of water contents and melt fractions consistent with a bulk conductivity of 1 S/m at a depth of 15 km below sea level (bsl) ( $P = 6 \text{ kbar}$ ). At these temperatures and pressures the observed conductivity anomaly cannot be explained by dry or moderately water-enriched ( $<6 \text{ wt.}\%$ ) andesite melts even when considering the unlikely scenario of a reservoir containing 100% melt. Evidently more than 6 wt%  $\text{H}_2\text{O}$  dissolved in the melt is need to explain the high conductivity of the APMB. At 6kbar, the  $\text{H}_2\text{O}$  solubility, defining the maximum melt water content in andesite, is around 10 wt.% ([Grove et al., 2012](#)), which requires a minimum melt fraction of 8% to explain the observed conductivity of the APMB ([Fig. 5](#)). However, if we consider saturation with a mixed  $\text{H}_2\text{O}-\text{CO}_2$  fluid, the maximum  $\text{H}_2\text{O}$  content in the melt is reduced; for example, with 15 mol%  $\text{CO}_2$  in the fluid, the maximum melt  $\text{H}_2\text{O}$  content is 7 wt.%, which would require a melt fraction of 45% in the APMB, corresponding to the maximum melt fraction of a rigid melt-crystal mush ([Fig. 5](#)).

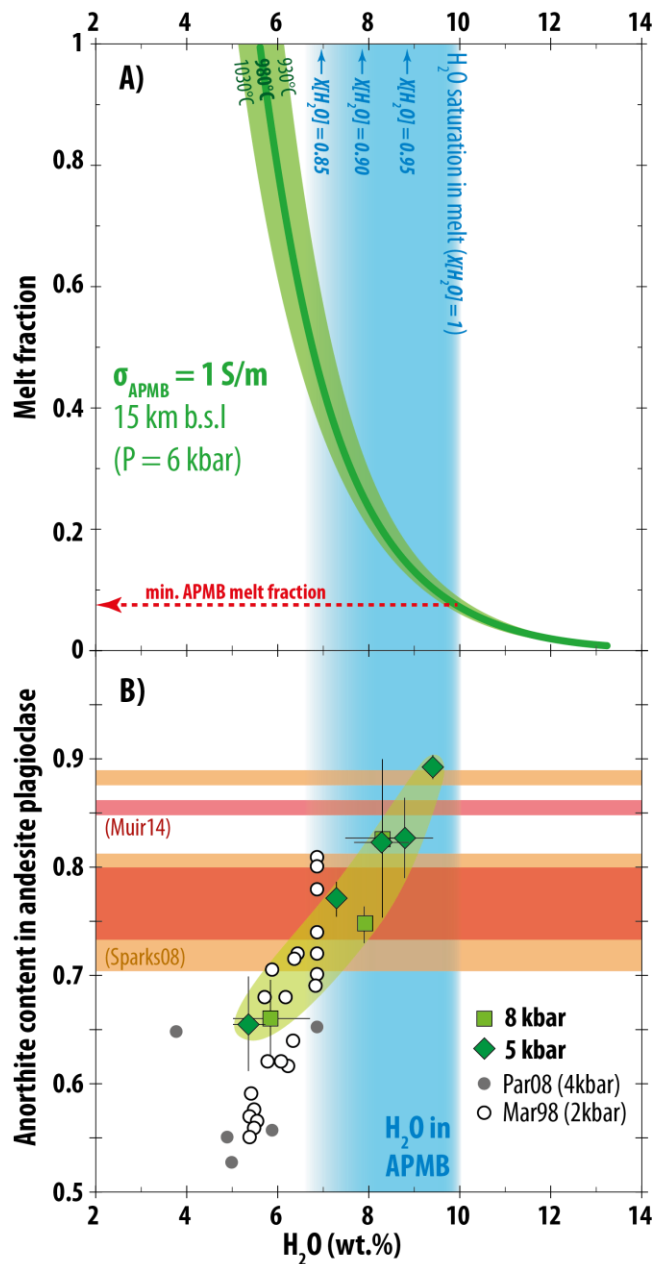


**Fig. 5. Determination of melt fraction and water content in APMB.** (A) Combinations of water content and melt fraction consistent with  $\sigma = 1 \text{ S/m}$  (Comeau et al., 2015) at depths > 15 km (6 kbar) below sea level. Pressure and temperature variations have negligible effect on the conductivity compared to water content and melt fraction. The minimum melt fraction is determined by the maximum water content at such depths (i.e. saturation), shown by the horizontal dashed line.  $X[\text{H}_2\text{O}]$  stands for the molar water fraction in the fluid phase. (B) Anorthite (An) content (An = molar Ca/Ca+Na) of plagioclase as a function of water content in andesite melt at temperatures ranging from 890 to 980°C and pressures of 5 – 8 kbar (Table 3), complemented by data from the literature (circles). Experimental data replicate the composition of natural plagioclase from Uturuncu andesitic enclaves (Sparks et al., 2008;

[Muir et al., 2014](#)) at dissolved water contents similar to those expected from geophysical data further strengthening the view that the APMB host andesitic melts.

The inferred high water content of the andesitic melts in the APMB can be independently corroborated using geochemistry and petrology. To this end, we use the high pressure phase equilibrium experiments on the Uturuncu andesite under water-saturated and undersaturated conditions, 5 to 8 kbar and 890-980 °C presented above. Our objective was to determine the conditions and water content of an andesitic melt that reproduce the observed liquidus phase assemblage and compositions in the Uturuncu andesite enclaves, *i.e.* phenocrysts of orthopyroxene, calcic plagioclase and Fe-Ti oxides with minor clinopyroxene and amphibole ([Sparks et al., 2008](#)). The experiments clearly demonstrate that the anorthite content (An) of plagioclase feldspar increases as  $H_2O_{\text{melt}}$  increases from 5 to 10 wt% irrespective of pressure and temperature (see [Fig. 5B](#) and [Table 3](#)). The experimental data of [Martel et al. \(1999\)](#) and [Parat et al. \(2008\)](#) extend this trend down to  $An_{55}$  at lower water contents. The high An content of plagioclase cores from the Uturuncu andesites ( $An_{>0.73}$ ) provides an exacting constraint on the andesite storage conditions. The natural liquidus mineral assemblage and plagioclase compositions ( $An_{0.75-0.83}$ ) were produced experimentally at 980°C, 5 and 8 kbar, in equilibrium with broadly andesitic residual glass containing 7 to 9 wt.% dissolved  $H_2O$  ([Fig. 5](#)). These independent constraints strongly indicate that the magma body at 15 to 30 km bsl contains 10-20 vol% of  $H_2O$  ( $\pm CO_2$ )-saturated andesitic melts at a temperature close to 980°C within a solid matrix, as suggested by the thermal models of [Annen et al. \(2006\)](#). The minimum melt water content must be 8 wt% in order to have Ca-rich plagioclase on the liquidus and to be sufficiently conductive. The petrological experiments corroborate the electrical conductivity model, providing a method to directly interpret the conductivity values obtained from MT data. In contrast to studying erupted lavas or exhumed plutonic rocks, both of which have degassed to various extents, our approach allows us to determine the present-day distribution and characteristics of melt in the crust.

The evolution of andesitic melt can produce more fractionated magmas after cooling down and crystallization. The residue left behind these fractionated liquids may be noritic cumulates (e.g. [Castro et al., 2013](#)) that remains filtered at the depth of the mid-lower crust. Fragments of norite cumulates can be found in the Uturuncu dacites ([Sparks et al., 2008](#)). We estimate that andesitic melt constitutes about 10 vol% of the APMB, the rest being composed of materials that remains invisible to MT sounding (low EC); noritic cumulates being long-produced by magmatic flare-ups, probably accompanied with a

mixture of the surrounding Andean crust (plus the accumulated solidified products of several millions of years of magmatism in this area) may constitute the remaining 90 vol% of the APMB. All in all, it must be clear that we can only address here the nature of the conductive materials in the APMB, the rest being “electrically” invisible. In our interpretation the andesite enclaves in Uturuncu dacites represent quenched droplets of the resident melt of the APMB. The dacite magmas themselves must be generated at or above the top of the APMB; their isotopic characteristics require mixing with a significant assimilation crustal melts in dacite petrogenesis, for which the andesites are plausible end-members (Michelfelder et al, 2014). However, further study is required to establish the exact proportions of crystal fractionation, mixing and crustal melting that are required to generate the Uturuncu dacites.

#### **4.1.2. Southern Washington Cascades Conductor**

Using the same methodology we investigated magma bodies detected beneath the Southern Washington Cascades Conductor (SWCC). In the Cascades, a large conductive body (0.1 to 1 S/m) was detected at ~20 km bsl and is thought to contain 2 to 12 vol% melts in the vicinity of Mount Rainier and Mount St. Helens (Hill et al., 2009; McGary et al., 2014). The synthesis of Wannamaker et al. (2014) showed that there is significant north-south variation in the conductivity structure of the Cascadia subduction zone, and that conductive anomalies extend down to the subducted slab in many places suggestive of flux melting of the mantle wedge. Magmas generated by this mechanism are likely basaltic, ascending and ponding in the crust to produce more evolved derivatives. Although these erupted lavas are dominantly felsic, they derive from intermediate magma as suggested by the andesitic products observed throughout the Cascades where andesite is understood to have been generated by polybaric differentiation from hydrous basaltic parents and stored at 980°C and depths >7 km (Kent et al., 2010; Pallister et al., 1992; Sisson & Grove, 1993). The process of differentiation increases the dissolved water content of derivative melts provided that pressure is sufficiently high to keep water in solution. The observed SWCC electrical conductor is consistent with the presence of 2-12 vol% of melt with  $8 \pm 2$  wt.% of water dissolved in the melt (Fig. 6), similar to dissolved water contents in melts of the APMB, and in keeping with inferences from experimental petrology (Grove et al., 2012 and reference therein). We propose that the hydrous basaltic magmas produced by fluxing the mantle wedge above the Cascadia Subduction Zone, as envisaged by Wannamaker et al. (2014), are the parents to andesites and more evolved rocks found throughout the Cascades. Differentiation of these basaltic occurs as they

ascend into the crust, pond and crystallize. As in the Altiplano, crustal melting and assimilation will also have played a part in generating the more evolved magmas of the Cascades.

#### 4.1.3. Taupo Volcanic Zone

Applying the same approach to the conductors imaged at depths of 10 - 25 km beneath the TVZ (Fig. 6) requires minimum water contents of 6 wt.% (most likely ~8 wt.%) in intermediate magmas (Hurst et al., 2016). This water content is slightly lower than for the SWCC or APMB magmas, consistent with shallower storage and, *de facto*, lower H<sub>2</sub>O solubility. Again, there is petrological support for such high water contents in the TVZ; Deering et al. (2011) propose that dacitic and silicic andesite melts from the ~10 ka Tongariro eruption contained 6.3±0.8 wt% H<sub>2</sub>O at a depth of 10 km. However, water-saturated intermediate magmas cannot explain the conductivity close to 1 S/m of shallower reservoirs (<10 km), which may thus be filled by more conductive, felsic magmas and/or magmatic brines associated with degassing of such magmas (Gaillard, 2004; Hurst et al., 2016).

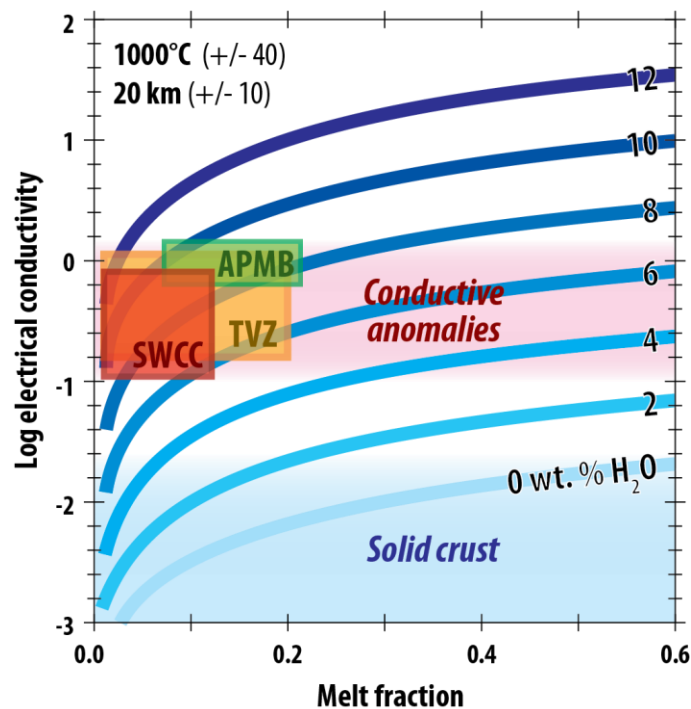


**Fig. 6. Electrical conductivity (Log scale, EC in S/m) of crustal magma bodies with respect to their melt fraction and water content.** Intermediate magma bodies located in the lower to mid crust must contain significant amounts of water (>6 wt.%) to produce the high conductivity observed by MT surveys. “Solid” crust corresponds to adjacent regions with low amounts of melt and water.

#### 4.2. Importance of water in the continental crust growth

Water-rich andesite melt reservoirs appear to be an important feature of the mid-crust in three continental subduction-zone settings. The depth of andesite melt storage within the APMB and the SWCC (15 to 20 km bsl) can be explained by their high dissolved H<sub>2</sub>O contents (>8 wt.%): ascent of the andesite to shallower depth would lead to H<sub>2</sub>O degassing, driving substantial crystallization (Lee & Bachmann, 2014; Annen et al., 2006; Sisson & Grove, 1993; Blundy & Cashman, 2001), impeding further magma ascent since crystallization increases the viscosity of magma. Water dissolved in magmas largely governs the ponding level where they differentiate and the attendant phase relations. Hence water is critical for understanding construction of continental crust (Annen et al., 2006; Plank et al., 2013; Jagoutz & Kelemen, 2015). At a broader scale, this can explain why intrusive magmatism dominates in arcs settings compared to the extrusive volcanism at drier hot spot and mid ocean ridge magmatism (Keller et al., 2015). We show that regardless of the compositional spectrum of erupted products, the dominant melt phase in the arc at mid-crustal depths is hydrous andesite in composition. Our approach is unable to establish whether arc andesites are the products of direct mantle melting (Castro et al., 2013) or crystallisation of mantle-derived basalts. The latter option would require parental basalts with ~4 wt.% H<sub>2</sub>O (Plank et al., 2013). The inferred dissolved water content of arc andesites reported in this study are at the upper end of that previously reported (Carmichael, 2002, Annen et al., 2006), further emphasizing the important role of the “andesite aqueduct” in the geologic water cycle and deep differentiation of arc magmas.

If the total APMB volume is taken to be 500,000 km<sup>3</sup> (Ward et al., 2014), then the mass of water contained in the reservoir is about 1.4x10<sup>16</sup> kg, which is comparable to the volume of the largest freshwater lakes on Earth. Considering a global flux of subducted water of 1.8.10<sup>15</sup> g/yr (Jarrard, 2003), the amount of water stored within the APMB corresponds to the amount of water subducted in ~ 6 Ma along a 100 km segment of a subduction zone. Therefore, the water content of the APMB either reflects the longevity of such crustal magma bodies or a subduction zone with an anomalously high flux of slab-derived water. The flux of water in other subduction loci remains to be determined so as to infer whether super-hydrous, deep magma reservoirs define the rule or constitute local anomalies for the growth of continental crust.

## 5. Conclusions

Our experiments show that the amount of dissolved water greatly impacts the electrical conductivity of andesitic melt at conditions encountered in the continental crust. We interpret the high

conductivities detected by MT studies of large, crustal magma reservoirs in subduction settings as being due to the presence of super-hydrous andesitic melts ( $\geq 8$  wt% H<sub>2</sub>O). This conclusion is supported by petrological evidence that arc magmas differentiate from hydrous, mantle derived basalts with  $\geq 4$  wt% H<sub>2</sub>O (Plank et al., 2013). Crystallization of such parents by roughly 50-60% to produce derivative andesite melts with  $\sim 60$  wt% SiO<sub>2</sub> at 1000 °C (e.g. Nandedkar et al., 2014) will involve a near doubling of the water content provided that pressures are sufficiently high to keep this water in solution, *i.e.* differentiation occurs in the mid to deep crust as envisaged by the hot zone concept of Annen et al. (2006). Our findings are also consistent with the high intrusive:extrusive ratio of magma in arc settings, and with the bulk chemical composition of continental crust. Depending on the abundance and distribution of such reservoirs, the water budget at active continental arcs may need to be reconsidered.

#### References:

- Annen, C., Blundy, J., Sparks, R.S.J. (2006). The genesis of intermediate and silicic magmas in deep crustal hot zones. *Journal of Petrology* **47**, 505-539.
- Blatter, D.L., Sisson, T.W., Hanks, W.B. (2013). Crystallization of oxidized, moderately hydrous arc basalt at mid- to lower-crustal pressures: implications for andesite genesis. *Contribution to Mineralogy and Petrology* **166**, 861-886.
- Blundy, J., Cashman, K.V. (2001). Ascent-driven crystallisation of dacite magmas at Mount St. Helens, 1980-1986. *Contributions to Mineralogy and Petrology* **140**, 631-650.
- Blundy, J., Cashman, K.V., Rust, A., Witham, F. (2010). A case for CO<sub>2</sub>-rich magmas. *Earth and Planetary Science Letters* **290** (3), 289-301.
- Boyd, F. England, J. (1960). Apparatus for phase-equilibrium measurements at pressures up to 50 kilobars and temperatures up to 1750°C. *Journal of Geophysical Research* **65** (2), 741-748.
- Carmichael, I. (2002). The andesite aqueduct: perspectives on the evolution of intermediate magmatism in west-central (105-99°W) Mexico. *Contribution to Mineralogy and Petrology* **143**, 641-663.
- Castro, A., Vogt, K., Gerya, T. (2013). Generation of new continental crust by sublithospheric silic-magma relamination in arcs: A test of Taylor's andesite model. *Gondwana Research* **23** (4), 1554-1566; DOI:10.1016/j.gr.2012.07.004.
- Comeau, M.J., Unsworth, M. J., Ticona, F., Sunagua, M. (2015). Magnetotelluric images of magma distribution beneath Volcán Uturuncu, Bolivia: Implications for magma dynamics. *Geology* **43**, 243-246. doi: 10.1130/G36258.1.
- Deering, C.D., Bachmann, O., Dufek, J., Gravley, D.M. (2011). Rift-related transition from andesite to rhyolite volcanism in the Taupo Volcanic Zone (New Zealand) controlled by crystal-melt dynamics in mush zones with variable mineral assemblage. *Journal of Petrology* **52** (11), 2243-2263.

- del Potro, R., Diez, M., Blundy, J., Camacho, A.G., Gottsmann, J. (2013). Diapiric ascent of silicic magma beneath the Bolivian Altiplano. *Geophysical Research Letters* **40**, 2044-2048.
- Edmonds, M., Humphreys, M.C.S., Hauri, E.H., Herd, R.A., Wadge, G., Rawson, H., Ledden, R., Plail, M., Barclay, J., Aiuppa, A., Christopher, T.E. (2014). Pre-eruptive vapour and its role in controlling eruption style and longevity at Soufrière Hills Volcano. *Geological Society, London, Memoirs* **39** (1), pp.291-315.
- Gaillard, F. (2004). Laboratory measurements of electrical conductivity of hydrous and dry silicic melts under pressure. *Earth and Planetary Science Letters* **218** (1), 215-228.
- Gaillard, F., Iacono-Marziano, G. (2005). Electrical conductivity of magma in the course of crystallization controlled by their residual liquid composition. *Journal of Geophysical Research: Solid Earth (1978–2012)* **110** (B6).
- Glover, P.W.J., Hole, M. J., Pous, J. (2000). A modified Archie's law for two-conducting phases, *Earth Planet. Sci. Lett.*, **180**, 369– 383.
- Green, D.H., Ringwood, A.E. (1967). An experimental investigation of the gabbro to eclogite transformation and its petrological applications. *Geochemica and Cosmochimica Acta* **31** (5), 767-833.
- Grove, T.L., Till, C.B., Krawczynski, M.J. (2012). The role of H<sub>2</sub>O in subduction zone magmatism. *Annual Review of Earth and Planetary Sciences* **40**, 413-439.
- Heise, W., Caldwell, T.G., Bibby, H.M., Bennie, S.L. (2010). Three-dimensional electrical resistivity image of magma beneath an active continental rift, Taupo Volcanic Zone, New Zealand. *Geophysical Research Letter* **37**, L10301, doi:10.1029/2010GL043110, 2010.
- Hill, G.J., Caldwell, T.G., Heise, W., Chertkoff, D.G., Bibby, H.M., Burgess, M.K., Cull, J.P., Cas, R.A.F, (2009). Distribution of melt beneath Mount St Helens and Mount Adams inferred from magnetotelluric data. *Nature Geoscience* **2**, doi:10.1038/NGEO661.
- Hurst, T., Heise, W., Hreinsdottir, S., Hamling, I. (2016). Geophysics of the Taupo Volcanic Zone: A review of recent developments. *Geothermics* **59**, 188-204.
- Jagoutz, O., Kelemen, P.B., (2015). Role of arc processes in the formation of continental crust. *Annual Review of Earth and Planetary Sciences* **43**, 363-404.
- Jakobsson, S. (2012). Oxygen fugacity control in piston-cylinder experiments. *Contributions to Mineralogy and Petrology* **164** (3), 397–406.
- Jarrard, R.D. (2003). Subduction fluxes of water, carbon dioxide, chlorine, and potassium. *Geochemistry Geophysics Geosystems* **4** (5), 8905, doi:10.1029/2002GC000392.
- Keller, C.B., Schoene, B., Barboni, M., Samperton, K.M., Husson, J.M., (2015). Volcanic-plutonic parity and the differentiation of the continental crust. *Nature* **523**, 301-307.
- Kent, A.J.R, Darr, C., Koleszar, A.M., Salisbury, M.J., Cooper, K.M., (2010). Preferential eruption of andesitic magmas through recharge filtering. *Nature Geoscience* **3**, doi:10.1038/NGEO924.
- Laumonier, M., Scaillet, B., Pichavant, M., Champallier, R., Andújar J., Arbaret, L. (2014). On the conditions of magma mixing and its bearing on andesite production in the crust. *Nature communications* **5**, doi:10.1038/ncomms6607.

- Laumonier, M., Gaillard, F., Sifre, D. (2015). The effect of pressure and water concentration on the electrical conductivity of dacitic melts: Implication for magnetotelluric imaging in subduction areas. *Chemical Geology* **418**. doi:10.1016/j.chemgeo.2014.09.019.
- Lee, C. T. A., Bachmann, O. (2014). How important is the role of crystal fractionation in making intermediate magmas? Insights from Zr and P systematics. *Earth and Planetary Science Letters* **393**, 266-274.
- McDade, P., Wood, B., Van Westrenen, W., Brooker, R., Gudmundsson, G., Soulard, H., Najorka, J., Blundy, J. (2002). Pressure corrections for a selection of piston-cylinder cell assemblies. *Mineralogical Magazine* **66** (6), 1021–1028.
- McGary, R.S., Evans, R.L., Wannamker, P.E., Elsenbeck, J., Rondenay, S. (2014). Pathway from subducting slab to surface for melt and fluids beneath Mount Rainier. *Nature Geoscience* **511**, doi:10.1038/nature13493.
- Martel, C., Pichavant, M., Holtz, F., Scaillet, B. (1999). Effects of fO<sub>2</sub> and H<sub>2</sub>O on andesite phase relations between 2 and 4 kbar. *J. Geophys. Res.* **104**, 29453-29470.
- Melekhova, E., Annen, C., Blundy, J. (2013). Compositional gaps in igneous rock suites controlled by magma system heat and water content. *Nature Geoscience* **6**, 385-390 doi:10.1038/ngeo1781.
- Maury, R. (1968). Conductibilité électrique des tectosilicates. I Méthode et résultats expérimentaux. *Bulletin de la Société Française de Minéralogie et Cristallographie* **91**, 355-366.
- Michelfelder, G.S., Feeley, T.C., Wilder, A.D. (2014). The Volcanic Evolution of Cerro Uturuncu : A High-K, Composite Volcano in the Back-Arc of the Central Andes of SW Bolivia. *International Journal of Geosciences* **5** (11), 1263.
- Muir, D., Blundy, J., Rust, A.C., Hickey, J. (2014a). Experimental constraints on dacite pre-eruptive magma storage conditions beneath Uturuncu volcano. *Journal of Petrology* **55**, 749-767.
- Muir, D., Blundy, J., Hutchinson, M., Rust, A.C. (2014b). Petrological imaging of an active pluton beneath Cerro Uturuncu, Bolivia. *Contributions to Mineralogy and Petrology* **167** (3), 1-25.
- Muir, D., Barfod, D., Blundy, J., Rust, A.C., Sparks, R.S.J., Clarke, K. (2015). The temporal record of magmatism at Cerro Uturuncu, Bolivian Altiplano, In Chemical, Physical and Temporal Evolution of Magmatic Systems, *Geological Society Special Publication* **422** doi: 10.1144/SP422.1.
- Nandedkar, R.H., Ulmer, P., Müntener, O., (2014). Fractional crystallisation of primitive, hydrous arc magmas: an experimental study at 0.7 GPa. *Contribution to Mineralogy and Petrology* **167** (6), 1-27.
- Ohlhorst, S., Behrens, H., Holtz, F. (2001). Compositional dependence of molar absorptivities of near-infrared OH-and H<sub>2</sub>O bands in rhyolitic to basaltic glasses. *Chemical Geology* **174** (1), 5-20.
- Pallister, J.S., Hoblitt, R.P., Crandell, D.R., Mullineaux, D.R. (1992). Mount St Helens a decade after the 1980 eruptions: magmatic models, chemical cycles, and a revised hazards assessment. *Bulletin of Volcanology* **54**, 126-146.
- Parat, F., Holtz, F., Feig, S. (2008). Pre-eruptive conditions of the Huerto Andesite (Fish Canyon system, San Juan volcanic field, Colorado): Influence of volatiles (COHS) on phase equilibria and mineral composition. *Journal of Petrology* **49**, 911-935.

- Plank, T., Kelley, K.A., Zimmer, M.M., Hauri, E.H., Wallace, P.J. (2013). Why do mafic arc magmas contain ~4wt% water on average?. *Earth and Planetary Science Letters* **364**, 168-179.
- Pommier, A., Gaillard, F., Pichavant, M., Scaillet, B. (2008). Laboratory measurements of electrical conductivities of hydrous and dry Mount Vesuvius melts under pressure. *Journal of Geophysical Research* **113** (B05205), doi:10.1029/2007JB005269.
- Pommier, A. (2014). Interpretation of Magnetotelluric Results using Laboratory measurements. *Surv. Geophys.* **35**, 41-84 ; DOI 10.1007/s10712-013-9226-2.
- Reubi, O., Blundy, J., (2009). A dearth of intermediate melts at subduction zone volcanoes and the petrogenesis of arc andesite. *Nature* **461**, 1269-1273.
- Rudnick, R. L. (1995). Making continental crust. *Nature* **378**, 571–578.
- Sisson, T.W., Grove, T.L. (1993). Temperatures and H<sub>2</sub>O contents of low-MgO high-alumina basalts. *Contributions to Mineralogy and Petrology* **113**(2), 167-184.
- Sifré, D., Gardés, E., Massuyeau, M., Hashim, L., Hier-Majumder, S., Gaillard, F. (2014). Electrical conductivity during incipient melting in the oceanic low-velocity zone. *Nature* **509**, 81-85.
- Sparks, R.S.J., Folkes, C.B., Humphreys, M.C.S., Barfod, D.N., Clavero, J., Sunagua, M.C., McNutt, S.R., Pritchard, M.E. (2008). Uturuncu volcano, Bolivia: Volcanic unrest due to mid-crustal magma intrusion, *American Journal of Science* **308**, 727-769.
- Wannamaker, P.E., Evans, R.L., Bedrosian, P.A., Unsworth, M.J., Maris, V., McGary, R.S. (2014). Segmentation of plate coupling, fate of subduction fluids, and modes of arc magmatism in Cascadia inferred from magnetotelluric resistivity. *Geochemistry, Geophysics, Geosystems* **15** (11), 4230-4253.
- Ward, K.M., Zandt, G., Beck, S.L., Christensen, D.H., McFarlin, H. (2014). Seismic imaging of the magmatic underpinnings beneath the Altiplano-Puna volcanic complex from the joint inversion of surface wave dispersion and receiver functions. *Earth and planetary science letter* **404**, 43-54.
- Zandt, G., Leidig, M., Chmielowski, J., Baumont, D., Yuan, X. (2003). Seismic detection and characterization of the Altiplano-Puna magma body, central Andes. *Pure and Applied Geophysics* **160**, 789-807.

**Acknowledgments:** This work benefitted from the help of H. Keppler for FTIR measurements and I. Di Carlo and D. Krause for EMPA analyses. ML was supported by ERC grant #279790, BGI visitor program and the Alexander von Humboldt Foundation. FG acknowledges the ERC #279790 and ANR #2010 BLAN62101 projects. DM was supported by the Natural and Environmental Research Council (NE/G01843X/1). JB acknowledge ERC Advanced Grant CRITMAG and Wolfson Research Merit Award from the Royal Society. MJU acknowledges support through an NSERC Discovery Grant and NSF grant EAR-0908281 to Cornell University. The authors thank A. Castro and an anonymous reviewer who helped in clarifying the manuscript, and J.P Brodholt for editorial assistance.